Journal of Geochemical Exploration 161 (2016) 85–97

Contents lists available at ScienceDirect

Journal of Geochemical Exploration

journal homepage: www.elsevier.com/locate/gexplo

Minerals of the Ag–Bi–Cu–Pb–S system from the Amensif carbonate-replacement deposit (western High Atlas, Morocco)

Said Ilmen [a,*], Abdelkhalek Alansari [a], Bouchra Baidada [a], Lhou Maacha [b], Amine Bajddi [b]

[a] Department of Geology, Faculty of Science-Semlalia, Cadi Ayyad University, 40000 Marrakech, Morocco
[b] Managem Mining Company (SA), Twin Center, 20330 Casablanca, Morocco

ARTICLE INFO

Article history:
Received 14 May 2015
Revised 20 September 2015
Accepted 16 November 2015
Available online 18 November 2015

Keywords:
Carbonate-replacement
Ag–Bi–Te sulphosalts
Base-metal sulphides
Lead isotope
Amensif
Western High Atlas
Morocco

ABSTRACT

The Amensif Cu–Pb–Zn–Ag-(Au) deposit is located on the northern flank of the western High Atlas Mountains, Morocco. This carbonate-replacement deposit occurs predominantly in Lower Cambrian carbonates along a major detachment fault that separates the Basal unit from the Upper unit. Orebodies are mainly massive replacements of carbonate strata, although sulphides also occur in veins. Silicification, chloritization, local skarn formation and sulphidation are the most important hydrothermal alteration features observed.

The mineralogy is dominated by base metal sulphides with subordinate sulphosalts of Ag, Bi, Sb, Pb, and Au. The ore consists of chalcopyrite, pyrite, galena, sphalerite, arsenopyrite, tetrahedrite, tennantite, and Bi–Ag–Sb–Cu–Pb–Te sulphosalts (matildite, schirmerite, native bismuth, bismuthinite, freibergite, hedleyite, and krupkaite), anglesite, covellite, malachite, and azurite. Silver commonly occurs as Ag–Bi–Sb–Pb sulphosalts intimately associated within galena. SEM analyses confirm the occurrence of invisible gold within sulphides. Although SEM analysis of auriferous sulphides indicates the presence of gold in sufficient quantities to explain the bulk gold concentrations; native gold has not been detected in our polished sections. Gangue minerals include predominantly chlorite, epidote, tremolite, calcite, Mn-dolomite, saddle dolomite, quartz, sericite, with minor andradite and vesuvianite. The presence of a bismuth association at the Amensif deposit is typical, and was effective in scavenging gold and silver. Lead isotope compositions of galena sampled from two regions in western High Atlas (Amensif and Tighardine) show a wide range in $^{206}Pb/^{204}Pb$ (18.053–18.324), $^{207}Pb/^{204}Pb$ (15.534–15.577) and $^{208}Pb/^{204}Pb$ (37.780–37.986). The Pb isotope signature suggests that Pb–Cu–Zn minerals were leached from the older reservoir of the Cambro–Ordovician volcano-sedimentary rocks during the Permian granite event. The Amensif deposit is a typical example of a distal skarn, and is compatible with a model for polymetallic carbonate-replacement type mineralization.

Contents

* Corresponding author.
E-mail address: said.ilmen@edu.uca.ma (S. Ilmen).

http://dx.doi.org/10.1016/j.gexplo.2015.11.008
0375-6742/

1. Introduction

The association among Bi, Au, Ag, Te, Cu, and Pb has been extensively documented in numerous types of mineralization worldwide including intrusion-related Au, stringer zones of VMS deposits, orogenic gold, skarns, carbonate-replacement Pb–Zn–Cu–Ag–Au deposits, etc. (Einaudi and Burt, 1982; Arribas, 1995; Marcoux et al., 1996; Meinert et al., 2003; Ciobanu and Cook, 2004; Cepedal et al., 2006; Ciobanu et al., 2006, 2010; Damian et al., 2008; Voudouris et al., 2008, 2013; Fornadel et al., 2011; Ye et al., 2014; Bristol et al., 2015). Gold and silver are intimately associated with Bi-chalcogenides in various ore deposits (Ciobanu et al., 2009) and with Bi–Te–Pb–Cu–Sb-bearing minerals in other ore deposits (Boyle and Jonasson, 1984; Cook, 1997; Cook and Ciobanu, 2004; Voudouris et al., 2013).

The presence of Bi-bearing minerals in the western High Atlas district was, however, recognized more recently. The first documented occurrence of Bi-sulphosalts was described by Baidada (2012) and Ilmen et al. (2014a) in an auriferous shear zone from the Talat n'Imjjad area. The explored Talat n'Imjjad shear zone contains native bismuth, bismuthinite, emplectite, wittichenite, tsumoite, laitakarite and other base metals such as chalcopyrite, pyrite, and sphalerite. The gold from the Talat n'Imjjad shear zone is documented in close association with the Bi–Cu assemblages. At the Tameksaout occurrence, Ilmen (2014-Unpublished work) has discovered the presence of Bi–Te–Ag minerals (tsumoite, freibergite, native silver) in close association with chalcopyrite, galena, and sphalerite.

The Amensif deposit is located within the northern side of the western High Atlas. It is considered a polymetallic carbonate-replacement deposit (Ilmen et al., 2014b). Major characteristics of field relations, mineralization, and hydrothermal alteration, have been described by Ilmen et al. (2014b). The recently discovered Bi–Ag–Au–Te minerals give the deposit additional interest; this paper constitutes the first confirmed report of Bi-sulphosalts in the Amensif deposit. Herein, we briefly describe characteristics of the mineralization, with a focus on the Bi–Ag–Te–Pb–Cu–(Au) minerals.

2. Regional geology

The metallogenic district of Guedmiwa belongs to the northern range of the western High Atlas Mountains and includes base and precious metal mineralization as at the Azegour Mo–Cu–W skarn deposit (Permingeat, 1957; Zerhouni, 1988; El Khalile et al., 2014; Berrada et al., 2015), the Assif El Mal Pb–Zn–(Cu–Ag) vein deposit (Bouabdellah et al. 2009), the Erdouz Ag–Zn–Pb vein deposit (Badra, 1993), the auriferous shear zone of Talat n'Imjjad (Ilmen et al., 2014a), and the Cu–Pb–Zn–Ag–(Au) carbonate replacement deposit at Amensif (Ilmen et al., 2014b). The regional geology includes Lower to Middle Cambrian and Ordovician volcano-sedimentary formations consisting of carbonate strata (dolostone, limestone, and marble), schist, sandstone, greywacke, basalt, andesite, dacite, and trachyte (Pouclet et al., 2008). This Lower Paleozoic sequence is intruded by the Permian Azegour granite (271 ± 3 Ma; Mrini et al., 1992) and the Al Medinet quartz diorite, and is cut by a swarm of Permian rhyolitic dikes (Fig. 1).

Structurally, the western High Atlas was affected by three deformational events (D1, D2, D3) (Dias et al., 2011; Ilmen et al., 2014b). The Guedmiwa domain is delimited by large faults (several km in length) that have been active since Hercynian times (Fig. 1) (Labriki 1996; Dias et al. 2011; Ilmen et al., 2014a,b). These large faults delineate different blocks of which the remarkably triangular Erdouz bloc is delimited by an ENE-WSW dextral mega-shear zone (Erdouz fault) and a second WNW–ESE sinistral shear zone (Al Medinet fault) (Fig. 1). Both structures were responsible for producing the strong deformation and heterogeneity in this domain. The precious and base metal ore described in this contribution is located at the intersections of these all faults (Badra, 1993; Alansari et al., 2009; Bouabdellah et al., 2009; Ilmen et al., 2014a,b).

3. Local geology

Geotectonically, the Amensif deposit is in the western High Atlas. It is located about 85 km SW of Marrakech city and about 5 km south of the famous Azegour W–Mo–Cu mine (Fig. 1) (Permingeat, 1957). The deposit is positioned at the intersection of NE- and NW-trending tectonic belts, between the Erdouz and Al Medinet fault zones. Faults and fractures trend NNE–SSW to ENE–WSW and WNW–ESE to NW–SE (Fig. 3D). The host rocks comprise Lower Paleozoic volcano-sedimentary sequence (Fig. 3A and 3B), overthrust by Cretaceous sedimentary rocks.

The stratigraphy of the study area consists of a thick (about 600 m) (Badra, 1993; Labriki, 1996; Bouabdellah et al., 2009) Cambrian metasedimentary and volcaniclastic sequence, overthrust by Cretaceous sedimentary rocks (Fig. 2). The metasedimentary sequence was regionally affected by a regional low-grade, greenschist-facies metamorphism (Badra, 1993; Ilmen, 2011; Ilmen et al., 2014a).

Two stratigraphic units can be distinguished: a lower volcano-sedimentary unit and an upper pelitic unit.

- The Basal unit is composed of carbonate rocks (limestone, marble, dolostone) (Figs. 3A, 4A–B,) overlain by calcareous and pelitic schists and calc-schists. This lower unit is marked by alternating limestone beds and lenses, interlayered with calcareous schists, volcaniclastic rocks, lavas (Fig. 4C–D), and pyroclastic rocks. The unit is considered to be the Lower Cambrian in age analogues to similar with age relations of the same unit in the Anti-Atlas (Badra, 1993; Alansari et al., 2009; Ilmen, 2011; Ilmen et al., 2014b).
- The Upper unit is composed predominantly of sandstone and green schists. Similarly, this unit is attributed to a Middle Cambrian (Ilmen, 2011; Ilmen et al., 2014b).

North–south trending felsic dikes dip towards the east and crosscut the Lower and Middle Cambrian formations (Fig. 3C). They are glassy rocks consisting of plagioclase, biotite, interstitial quartz and phenocrysts of quartz (Fig. 4C). Based on their texture, mineralogical composition, and preliminary geochemical data, they can be classified as rhyolites.

4. Methods

Detailed geological and petrographic descriptions of twenty-five drill cores were used as the basis for sampling of altered and mineralized rocks at Amensif. More than 100 samples were collected from the surface and from cores in the mineralized intercepts for petrography, geochemical analysis and study by a scanning electron microscopy (SEM). Thirty thin sections and forty polished sections were prepared for petrographic observations at the DLGR laboratory, Cadi Ayyad University (Marrakech). ICP-AES analyses were carried out by using a Horiba Jobin Yvon ULTIMA 2c spectrometer. More than 100 ICP analyses for metals were performed at the Reminex Research Center and Laboratory (Marrakech). The bismuth-bearing associations are complex and hard to identify. Identification of all mineral phases, including opaque minerals, requires the use of SEM imagery and microanalysis. Six polished sections were studied using a Philips XL30 instrument equipped with SE, BSE and EDX detectors at the Reminex Research Center and Laboratory (Marrakech). Operating conditions included an accelerating voltage of 20 to 30 kV, a beam current of 20 nA and count times of 20 s. Ore minerals were analysed by ICP-AES and SEM–EDX for Fe, Cu, Pb, Zn, Au, Bi, and Se.

Lead isotope analyses were carried out on galena mineral separates that were hand-picked from two samples of ores in the Amensif Area. The two samples, one for Amensif deposit and one for Tighardine deposit, were analysed for Lead isotopic composition at the GEOTOP Laboratory-UQAM, Canada.

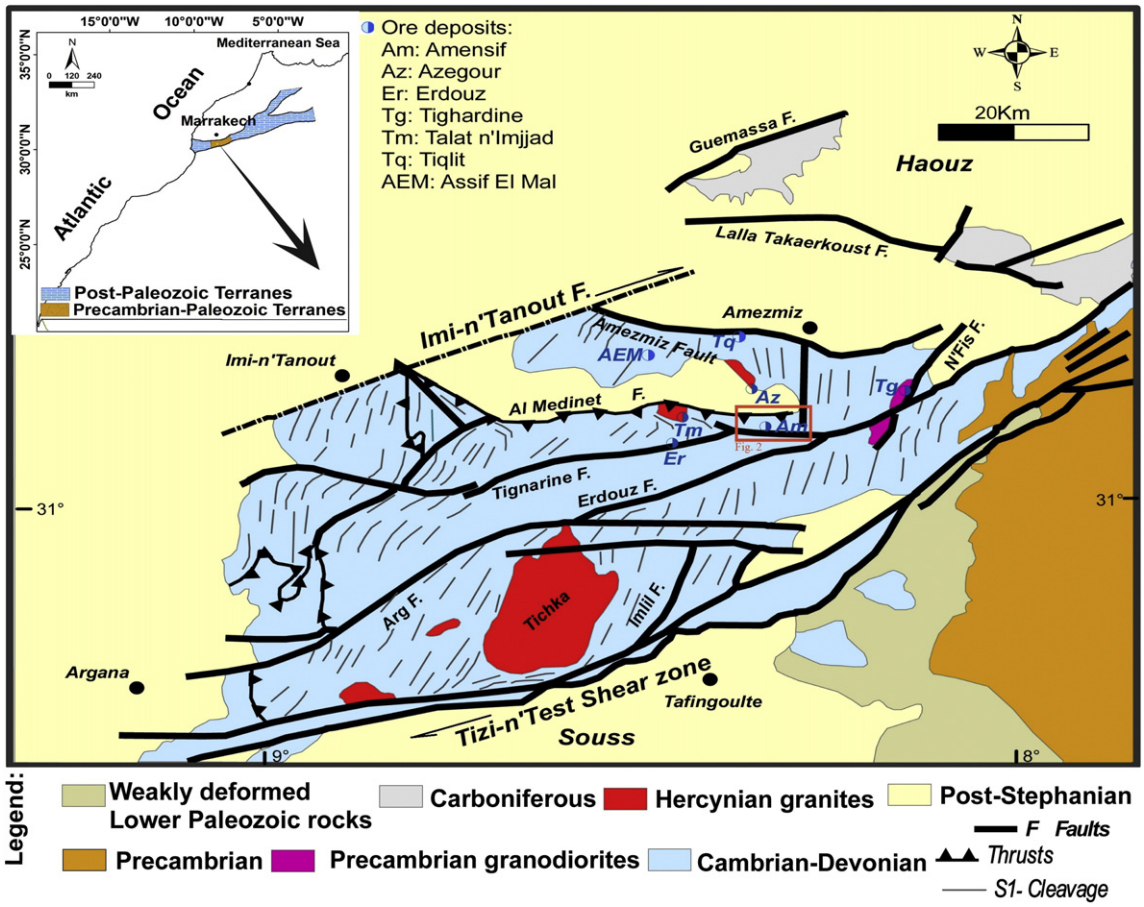

Fig. 1. Simplified geological map of the western High Atlas. The inset shows the location area into the Moroccan sketch (modified from Dias et al. 2011).

5. Results

5.1. Hydrothermal alteration

Hydrothermal alteration associated with the replacement deposit at Amensif is marked by silicification, chloritization, sericitization, and dolomitization. Local skarn formation in the host marbles is observed.

In the Amensif deposit, three main hydrothermal transformations are recognized, silicification, sericitization and hydrothermal dolomitization (Fig. 5). These alterations are responsible for the recrystallization of the limestone wall-rocks to various degrees (silicified limestones, marble). The microcrystalline calcite and dolomite of the limestones has been almost completely replaced by quartz as a result of an intense silicification (Fig. 5A, B, and C). The hydrothermal dolomitization is the last alteration phase developed and it is marked by recrystallization of limestones and development of saddle dolomite (Fig. 5B). Skarnification is relatively weak and it is limited to surface area of 20 m^2. It is present only in the immediate contact with rhyolitic dikes. This skarnification is marked by the development of anhydrous and hydrous skarn minerals. Anhydrous minerals are andradite (Fig. 5D) and vesuvianite characterizing the prograde alteration. Intense retrograde alteration is common in skarns (Einaudi and Burt, 1982; Meinert, 1992; Calagari and Hosseinzadeh, 2006; Canet et al., 2009; Ilmen et al. 2014b) and in some carbonate replacement deposits may destroy most of the prograde anhydrous calc-silicates (Cox, 1986; Morris, 1986). At Amensif, retrograde alteration is characterized by hydrous mineral assemblages composed of epidote + chlorite + tremolite + quartz + calcite + sericite minerals (Fig. 5E).

The main hydrothermal minerals identified are:

Quartz occurs as fine-medium grained (up to 0.8 mm across) patchy aggregates, solitary dispersed crystals and as veins and veinlets within the calc-silicates. Strong silicification has led to replacement of most former minerals by quartz.

Small amounts of sericite are observed with chlorite and quartz.

Dolomite occurs as fine hydrothermal grained to coarse 20–200 μm anhedral to subhedral crystals within the hydrothermal zones. Dolomite varies from dark grey to green. The micro- and pseudospar textures of the Amensif dolostone are replaced by closely packed anhedral saddle dolomite with undulatory extinction. Medium to coarse grained crystals (1 to 7 mm) are also present in veinlets cutting other mineral aggregates, where they show different texture and are accompanied by very fine to coarse crystals (1 to 10 mm) of dolomite and ankerite and sericite. Some carbonate minerals are partially and locally replaced by calc-silicate minerals. In comparison with non-altered dolomite, the hydrothermal dolomite occurs in coarse-crystalline euhedral rhombs, granular, massive and irregular forms. The intensity of dolomitization increases with increased depth.

Chlorite is very abundant, both in the mineralization, the footwall altered pelites and the carbonates. In the calc-silicate-rich units, it occurs as up to 350 μm-wide platelets that can form spherulitic aggregates, commonly in association with quartz, epidote, calcite and tremolite.

Epidote is the second most abundant component of the mineralization after chlorite, as it occurs in all the calc-silicate assemblages, in the sulphide mantos and in the footwall altered metasedimentary rocks of the foot-wall. Its main occurrence is as microcrystalline epidote-chlorite assemblages with quartz, calcite, andradite, tremolite and

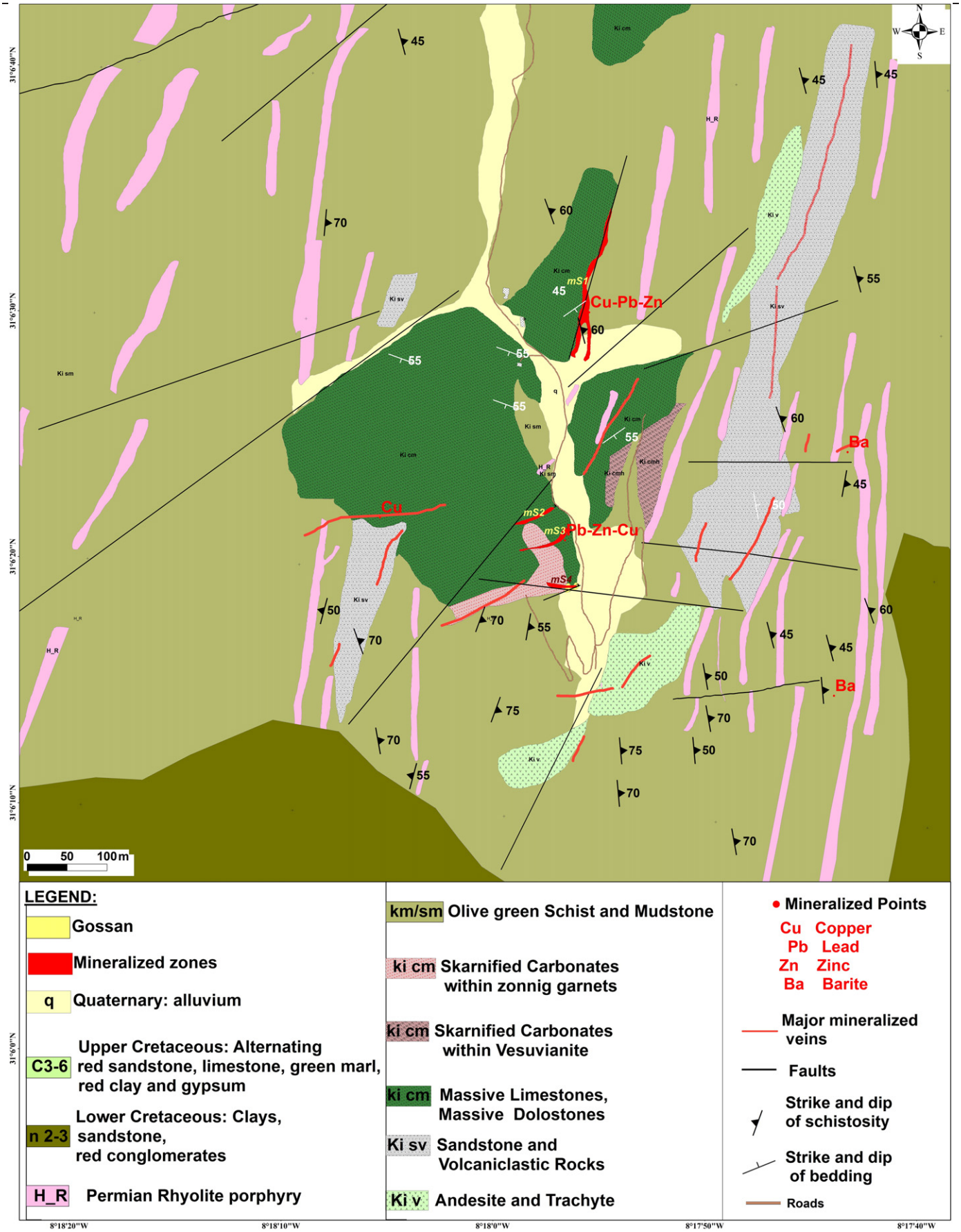

Fig. 2. Detailed geological map of Amensif deposit (Ilmen et al. 2014b). Legend: Ki (v, sv, cm): Lower Cambrian; Km/sm: Middle Cambrian; n2–3: Lower Cretaceous; C3–6: Upper Cretaceous; q: Quaternary.

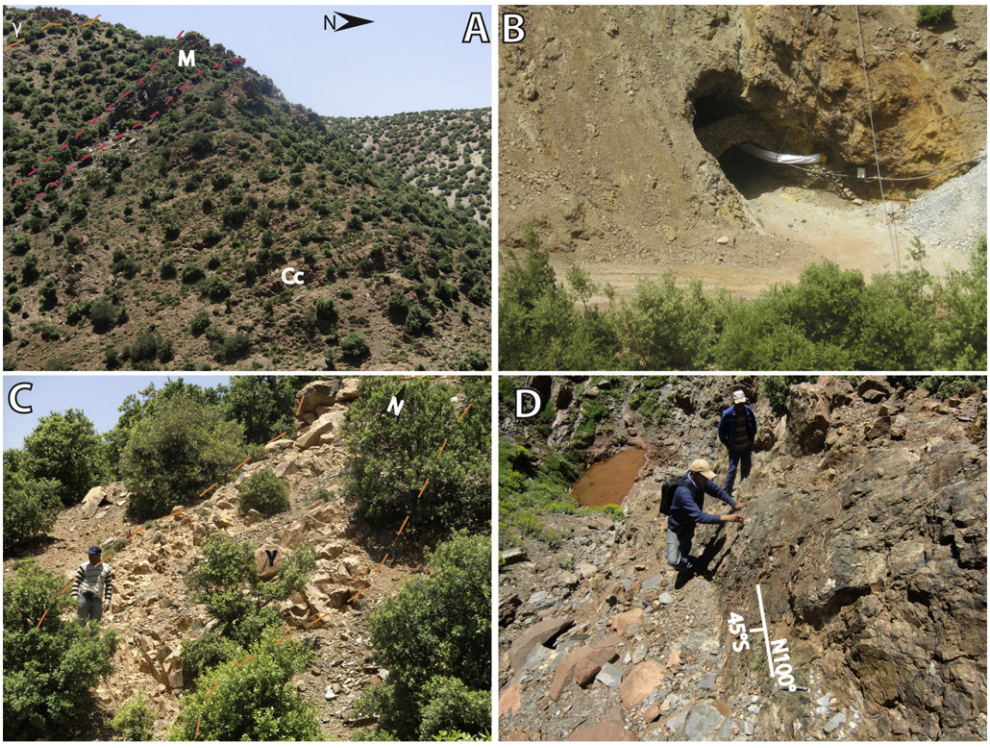

Fig. 3. Field photographs. A — photograph showing carbonate bars (cc) cut by mineralized structures (M) and by rhyolitic dikes (γ). B — photograph showing exploitation tunnel with gossan. C — N–S trending rhyolitic dike from Amensif. D — N100°-trending fault plane.

sulphides (chalcopyrite, galena, sphalerite and pyrite). Epidote occurs as euhedral prismatic crystals.

Tremolite occurs as spherulitic crystals commonly associated with chlorite, epidote and calcite. It is abundant in the footwall altered metapelites. Tremolite is partially replaced by chlorite.

Andradite: field and petrographic observations reveal a localized occurrence of garnet in marble and metamorphic limestones that are cross-cut by the rhyolitic dikes. Under the microscope, the garnet appears commonly as fine-grained subhedral forms. Crystals are as large as 5 to 7 mm in diameter. The petrographic characteristics and chemical

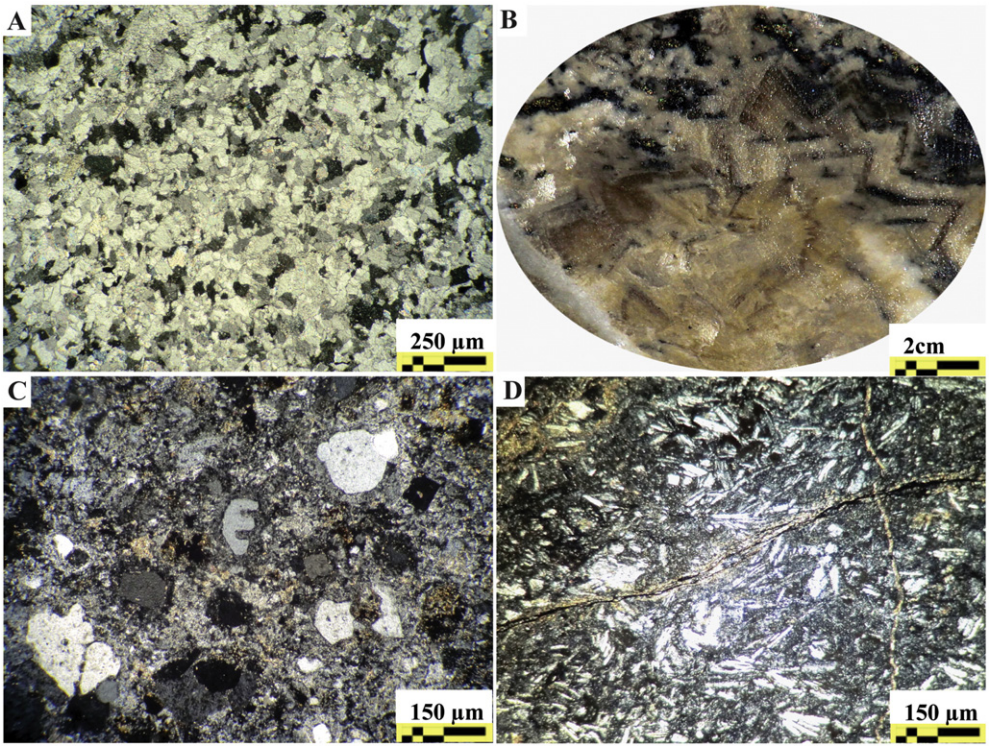

Fig. 4. A — photomicrograph showing medium to coarse grained fresh dolomite. B — photograph of saddle dolomite. C — microscopy texture of rhyolitic dike. D — trachytic texture of trachyte rocks.

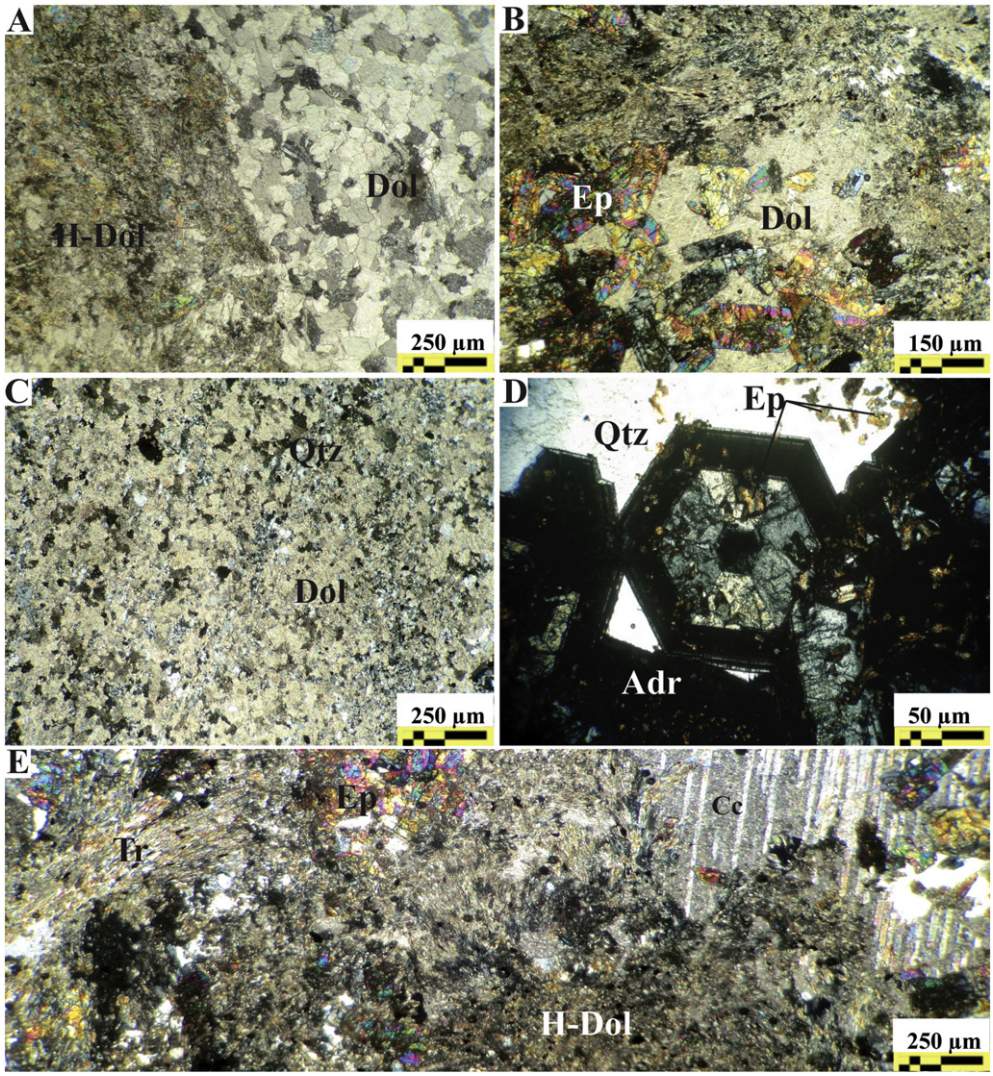

Fig. 5. A — photomicrograph showing contact between fresh dolomite and hydrothermal dolomite. B — hydrothermal dolomite with epidote (Ep) minerals. C — silicified dolomite. D — andradite (Adr) aggregates showing concentric-oscillating zoning with interstitial quartz (Qtz) and replaced by epidote (Ep). E — photomicrograph of hydrothermal dolomite (H-Dol) with anhydrous minerals: tremolite (Tr), epidote (Ep), and calcite (Cc).

composition of a garnet sample are consistent with andradite (Ca-rich garnet). Most of the andradite crystals observed in Amensif had coarse concentric-oscillating zoning and sector twins distinguished by colour and chemical composition. Andradite is associated with quartz, calcite, chlorite, epidote, pyrite, galena and chalcopyrite (Ilmen et al., 2014b).

Vesuvianite occurs mostly in metamorphic limestones as euhedral, randomly oriented prismatic phenocrysts a few tens of μm to 6 mm in size. XRF analysis confirmed the presence of association of F-rich vesuvianite associated with quartz and calcite (Ilmen et al., 2014b).

Barite occurs mostly in veins. Two types of barite are present in the Amensif deposit: the white barite and the pink barite. At −100 m underground, the white barite is associated with chalcopyrite, galena, and Fe-poor sphalerite.

5.2. Mineralization

The carbonate replacement orebodies in the Amensif area are irregular in shape and have vein-like extensions that follow faults and fissures. Massive sulphide bodies occur within the marbles and hydrothermal dolomites as well as along the contact of rocks with different permeabilities (carbonates, schists, greywackes, rhyolites). Schists are not mineralized. Two main types of sulphide mineralization are exposed in surface and underground workings. The most common ore type consists of massive sulphide replacement bodies hosted in Lower Cambrian carbonates (marbles, hydrothermal dolomites). The second type comprises lens-like (veins), disseminations, or semi-massive sulphide.

There is a close spatial relationship between felsic dikes (rhyolites) and ores, especially where limestones are cut by dikes. These dikes are enriched in base metals and oxidized in contact with the Lower Cambrian carbonates.

5.2.1. Mineralogy

The primary massive sulphide carbonate replacement ore is composed chiefly of chalcopyrite, sphalerite with chalcopyrite disease, galena, pyrite, arsenopyrite, tennantite-tetrahedrite and minor magnetite and pyrrhotite. SEM microscopy reveals the presence of Ag–Bi–Te–Sb–Pb–Cu minerals. Silver occurs mainly as silver sulphosalts, such as tetrahedrite, tennantite, freibergite, matildite, schirmerite and Ag–Au amalgam (Figs. 6 and 7, Tables 1, 2 and 3). The Bi-minerals show an intimate association with galena and consist mainly of Bi sulphosalts (bismuthinite, matildite, schirmerite, bismuthinite derivatives [hedleyite, krupkaite]), and native elements (native bismuth, Ag–Au amalgam). Oxidizing conditions favoured the formation of hypogene copper carbonates (malachite and azurite), lead sulphates (anglesite), and iron hydroxides (goethite and hematite). Detailed

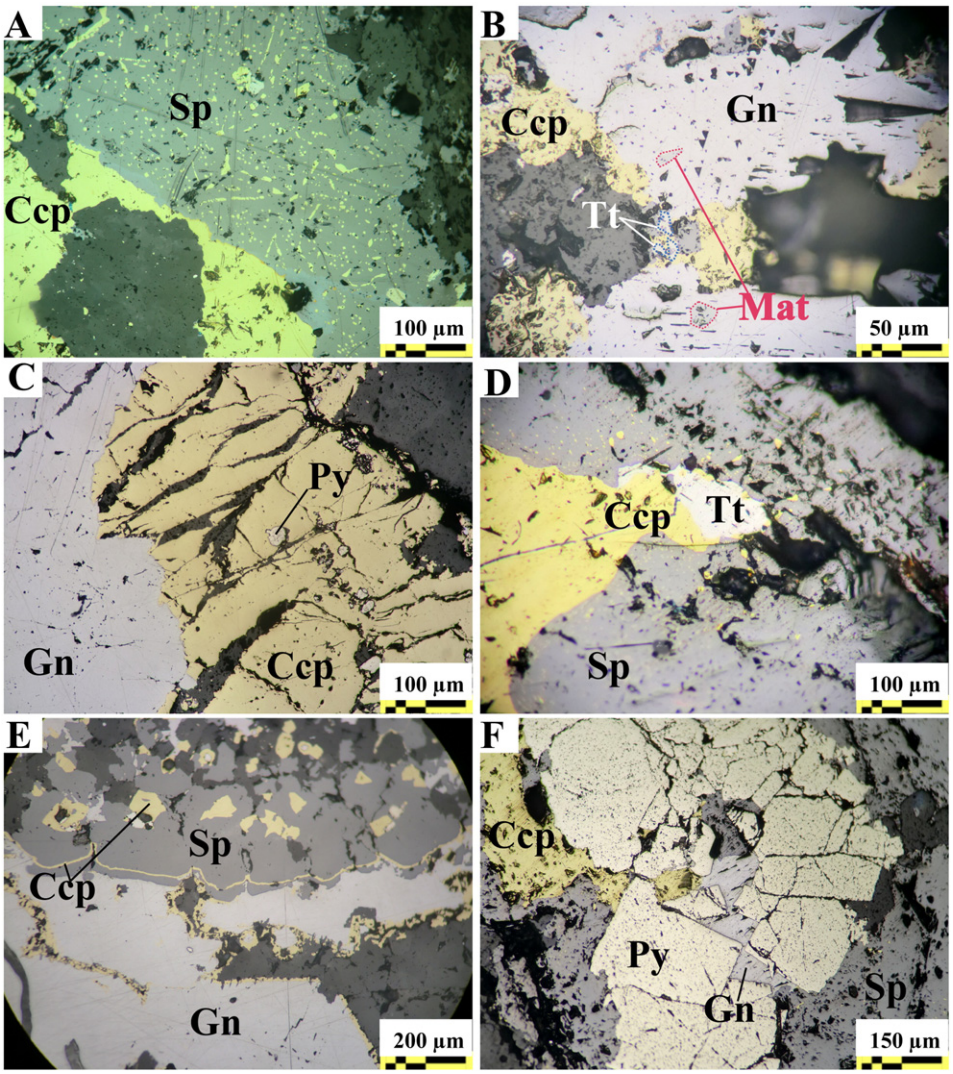

Fig. 6. Photomicrographs of mineralization. A — association of chalcopyrite (Cpy) and sphalerite (Sp) with chalcopyrite disease. B — association of chalcopyrite and galena (Gn) containing matildite (Mat), tennantite (Tt) forms on grain margins of chalcopyrite and galena. C — Brecciated pyrite (Py) replaced by chalcopyrite with is also replaced by galena. D — association of chalcopyrite, tennantite, and sphalerite. E — Replacement texture among sphalerite, chalcopyrite, and galena. F — fractures of pyrite filled by chalcopyrite and galena with association of sphalerite.

textural investigations of the ore assemblages reveal the presence of replacement textures among the sulphide minerals.

On the basis of optical microscopy and SEM observations, mineralogical characteristics of the Amensif deposit are shown below:

Chalcopyrite is a major phase in the main chalcopyrite-sphalerite-galena orebodies. It occurs as fine-coarse-grained crystals (>1 mm) and is present as interstitial disseminations or as patchy aggregates with mutual interference boundaries against the others main sulphides. Chalcopyrite is usually homogeneous (Fig. 6A, B, and D), but in some places contains very fine-grained replacements of sphalerite. Chalcopyrite is observed also forming some blebs in sphalerite. These blebs of chalcopyrite are called chalcopyrite disease (Fig. 6A) (Barton and Bethke, 1987). Microscopic examinations indicate the presence of tetrahedrite–tennantite closely associated with chalcopyrite.

Sphalerite occurs as massive, porphyritic, banded and disseminated aggregates commonly in association with chalcopyrite, galena, pyrite, arsenopyrite, quartz, calcite and other minerals. It is fine- to moderately coarse-grained and has a xenomorphic–subidiomorphic granular texture. Sphalerite varies in colour, but is commonly brown and brownish-yellow. Sphalerite is a ubiquitous sulphide in all the orebodies at Amensif and it is the most abundant ore mineral on a deposit scale. Sphalerite is also disseminated in the host-rock massive dolomite and in the carbonaceous dolomite. It contains a small oriented blebs and inclusions of chalcopyrite (chalcopyrite disease) (Fig. 6A). These blebs indicate high temperature co-genetic formation of chalcopyrite and sphalerite from a parent Cu–Zn–S solid solution (Barton and Bethke, 1987; Eldridge et al., 1988; Ramdohr, 1969). Eleven SEM–EDX analyses of sphalerite from the Amensif deposit (Table 3) show two types of sphalerite; Fe-rich sphalerite and Fe-poor sphalerite. The Fe-rich sphalerite contains 3.1 to 10.53 wt.% Fe, 38.13 to 42.46 wt.% S, and 49.29 to 58.77 wt.% Zn. The Fe-poor sphalerite is composed of 28.92 to 40.75 wt.% S and 59.25 to 71.08 wt.% Zn.

Pyrite is a major component of the ore characterizing the first ore stage. It occurs as aggregates and cubic crystals up to 0.6 mm across. Two generations of pyrite were distinguished at Amensif. The first one is formed during the early stage (I). It is typically euhedral and coarse-grained (1–3 mm) but also displays brecciated texture in late-stage fracture zones where it is entirely fractured and replaced by chalcopyrite (Fig. 6C), galena (Fig. 6F), and sphalerite formed during the late stage (II). Early stage pyrite is associated with arsenopyrite and quartz. The second generation of pyrite is attributed to the second or late stage of mineralization. It occurs as aggregates and intergrowths of micro-euhedral cubes within arsenopyrite. The textural relationships between pyrite and arsenopyrite indicate a co-genetic crystallization with a slight

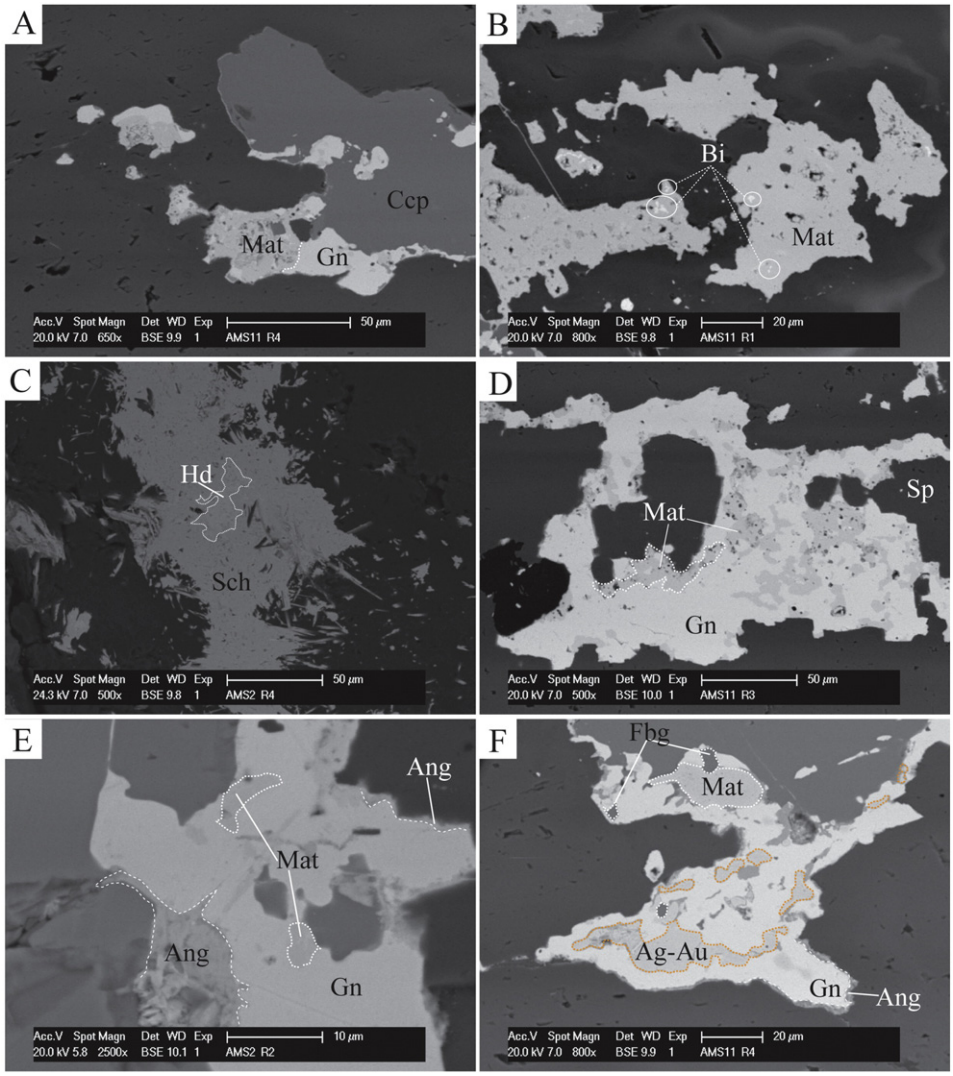

Fig. 7. BSE images. A — Association of chalcopyrite (Cpy), galena (Gn), and matildite (Mat). B — inclusions of native bismuth (Bi) in matildite. C — hedleyite (Hd) inclusion in schirmerite (Sch). D — matildite in galena associated with sphalerite (Sp). E — matildite inclusions in galena with rims replaced by anglesite (Ang). F — Ag–Au amalgam in close association with galena (with anglesite at rims), matildite, and freibergite.

Table 1
Chemical compositions (wt.%) of selected minerals from the Amensif deposit. (Analyses by SEM–EDS).

Mineral	Sample	S	Sb	Fe	As	Bi	Pb	Ag	Au	Zn	Cu	Te	O
Arsenopyrite	AMS-6′	26.94	2.74	33.28	37.04	–	–	–	–	–	–	–	–
	AMS-7/1	27.52	–	30.83	41.65	–	–	–	–	–	–	–	–
	AMS-2	19.02	–	31.56	49.43	–	–	–	–	–	–	–	–
	AMS-11	19.44	–	32.69	47.87	–	–	–	–	–	–	–	–
	AMS-11	19.38	–	29.91	50.71	–	–	–	–	–	–	–	–
Pyrite	AMS-6′	57.91	–	42.09	–	–	–	–	–	–	–	–	–
	AMS-6′	57.59	–	42.41	–	–	–	–	–	–	–	–	–
	AMS-7/1	58.14	–	41.86	–	–	–	–	–	–	–	–	–
	AMS-11	59.59	–	40.41	–	–	–	–	–	–	–	–	–
Chalcopyrite	AMS-6′	42.37	–	28.14	–	–	–	–	–	–	29.49	–	–
	AMS-6’	40.46	–	28.47	–	–	–	–	–	–	31.07	–	–
	AMS-7/1	41.6	–	28.65	–	–	–	–	–	–	29.75	–	–
	AMS-7/1	41.85	–	28.65	–	–	–	–	–	–	29.5	–	–
	AMS-8/2	42.56	–	28.22	–	–	–	–	–	–	29.22	–	–
	AMS-2	41.2	–	29.49	–	–	–	–	–	–	29.31	–	–
	AMS-11	44.51	–	27.9	–	–	–	–	–	–	27.59	–	–
	AMS-11	42.11	–	27.58	–	–	–	–	–	–	30.31	–	–
	AMS-11	42.69	–	28.16	–	–	–	–	–	–	29.15	–	–
Tennantite	AMS-7/1	31.79	4.77	3.85	12.49	–	–	12.15		7.25	27.7	–	–
Freibergite	AMS-11	25.3	22.77	5.38	–	–	–	32.74			13.81	–	–

Table 2
Chemical compositions (wt.%) of selected minerals from the Amensif deposit. (Analyses by SEM–EDS) (continuation).

Mineral	Sample	S	Sb	Fe	As	Bi	Pb	Ag	Au	Zn	Cu	Te	O
	AMS-2	16.09	–	–	–	55.3	–	28.61	–	–	–	–	–
	AMS-2	14.21	–	–	–	58.8	–	27	–	–	–	–	–
	AMS-2	15.34	–	–	–	59.19	–	25.48	–	–	–	–	–
	AMS-11	21.26	–	–	–	50.95	–	27.79	–	–	–	–	–
Matildite	AMS-11	16.55	–	–	–	52.37	–	31.08	–	–	–	–	–
	AMS-11	19.58	–	–	–	50.81	–	29.61	–	–	–	–	–
	AMS-11	20.49	–	–	–	52.52	–	26.99	–	–	–	–	–
	AMS-11	16.81	–	–	–	52.2	–	30.99	–	–	–	–	–
	AMS-11	16.54	–	–	–	55.72	–	27.74	–	–	–	–	–
	AMS-2	10.84	–	–	–	60.28	23.35	5.53	–	–	–	–	–
	AMS-2	12.94	–	–	–	61.52	18.7	6.84	–	–	–	–	–
Schirmerite	AMS-2	17.89	–	–	–	53.1	21.75	7.27	–	–	–	–	–
	AMS-2	20.9	–	–	–	40.62	29.9	8.58	–	–	–	–	–
	AMS-2	13.8	–	–	–	61.48	18.82	5.9	–	–	–	–	–
	AMS-2	13.64	–	–	–	59.5	21.12	5.74	–	–	–	–	–
Bismuthinite	AMS-2	13.7	–	–	–	86.3	–	–	–	–	–	–	–
Native Bismuth	AMS-2	–	–	–	–	100	–	–	–	–	–	–	–
Hedleyite	AMS-2	–	–	–	–	85.52	–	–	–	–	–	14.48	–
Krupkaite	AMS-2	12.91	–	–	–	60.79	22.73	–	–	–	3.57		–
	AMS-11	–	–	–	–	–	–	74.91	25.09	–	–	–	–
Ag–Au	AMS-11	–	–	–	–	–	–	69.59	30.41	–	–	–	–
	AMS-11	–	–	–	–	–	–	65.73	34.27	–	–	–	–

delay between the beginning of formation of arsenopyrite and that of pyrite. The latter was affected by a super-gene alteration and has been successively pseudomorphosed to goethite.

Arsenopyrite (FeAsS) occurs as euhedral rhombic crystals and forms aggregates within pyrite (Fig. 7B, D). It occurs in two generations at Amensif. The first one is characterized by monomineral aggregates of coarse-grained idiomorphic and is associated with coarse-grained pyrite formed during the first Fe–As ore-stage. During this stage, pyrite and arsenopyrite are affected by an intensively hydrothermal brecciation. Replacement of arsenopyrite is very common. The second generation of arsenopyrite is characterized by fine grain size and is associated with fine grained size of pyrite formed during the last ore stage (II).

Galena (PbS) occurs as moderately coarse-grained (0.5 to 15 mm), subidiomorphic–idiomorphic grains that typically occur as aggregates in coexistence with sphalerite, pyrite and calcite. Cubic crystals of galena are present. It is closely associated with sphalerite, chalcopyrite and pyrite (Fig. 6E). In the second ore stage, galena occurs as anhedral crystals filling cracks and fractures in pyrite formed during the first stage (Fig. 6F) but it is most abundant in metasomatic dolomite, where it forms aggregates with andradite and epidote. Microscopic observations and geochemical data indicate the presence of Bi–Ag-sulphosalts and tennantite as inclusions in galena crystals (Figs. 6B, 7A, B, D, E, and F).

According to SEM analyses (Table 3), in the absence of Ag and Bi, the galena is essentially pure PbS. When Ag and Bi are present, a solid solution of galena–matildite is formed. Our SEM imageries reveal the presence of exsolved matildite in galena.

Matildite ($AgBiS_2$) has been identified for the first time at the western High Atlas belt, based on SEM–EDX data and some X-ray powder-diffraction data (Alansari, unpublished). This mineral is present as exsolutions in galena (Fig. 6B). It forms with galena a solid solution of galena–matildite. According to Foord and Shawe (1989), the exsolutions of matildite from galena occurred below about 215 °C.

Table 3
Chemical compositions (wt.%) of selected minerals from the Amensif deposit. (Analyses by SEM–EDS) (continuation).

Mineral	Sample	S	Sb	Fe	As	Bi	Pb	Ag	Au	Zn	Cu	Te	O
Galena	AMS-6′	13.04	–	–	–	–	86.96	–	–	–	–	–	–
	AMS-6′	16.8	–	–	–	–	83.2	–	–	–	–	–	–
	AMS-6′	14.87	–	–	–	–	85.13	–	–	–	–	–	–
	AMS-7/1	14.11	–	–	–	–	85.89	–	–	–	–	–	–
	AMS-8/2	10.55	–	–	–	–	89.45	–	–	–	–	–	–
	AMS-8/2	10.71	–	–	–	–	89.29	–	–	–	–	–	–
	AMS-8/2	11.47	–	–	–	–	88.53	–	–	–	–	–	–
	AMS-2	13.21	–	–	–	–	86.79	–	–	–	–	–	–
	AMS-2	17.25	–	–	–	–	82.75	–	–	–	–	–	–
	AMS-2	13.41	–	–	–	–	86.59	–	–	–	–	–	–
	AMS-2	9.24	–	–	–	–	90.76	–	–	–	–	–	–
	AMS-11	7.75	–	–	–	–	92.25	–	–	–	–	–	–
	AMS-11	6.36	–	–	–	–	93.64	–	–	–	–	–	–
Anglesite	AMS-2	10.32	–	–	–	–	67.02	–	–	–	–	–	22.66
	AMS-2	10.26	–	–	–	–	68.68	–	–	–	–	–	21.06
Sphalerite	AMS-6′	39.8	–	3.62	–	–	–	–	–	56.57	–	–	–
	AMS-6′	4.23	–	4.3	–	–	–	–	–	55.48	–	–	–
	AMS-6′	38.13	–	3.1	–	–	–	–	–	58.77	–	–	–
	AMS-7/1	30.12	–	–	–	–	–	–	–	69.88	–	–	–
	AMS-7/1	28.92	–	–	–	–	–	–	–	71.08	–	–	–
	AMS-8/2	38.58	–	–	–	–	–	–	–	61.42	–	–	–
	AMS-8/2	40.75	–	–	–	–	–	–	–	59.25	–	–	–
	AMS-2	38.5	–	10.53	–	–	–	–	–	50.97	–	–	–
	AMS-2	38.99	–	7.42	–	–	–	–	–	53.59	–	–	–
	AMS-11	42.46	–	8.25	–	–	–	–	–	49.29	–	–	–
	AMS-11	29.98	–	–	–	–	–	–	–	70.02	–	–	–

Schirmerite ($Ag_3Pb_3Bi_9S_{18}$) occurs as medium to coarse grains (up to 30 μm) (Fig. 7C). Schirmerite is the second most abundant Bi-sulphosalts after matildite in the Amensif deposit.

Native bismuth (Bi) is observed as small inclusions in matildite, schirmerite, bismuthinite and in galena (Fig. 7B).

Investigation of polished sections through reflected light and SEM analyses show presence of Bismuthinite ($CuBiS_2$) in close association with schirmerite and matildite.

Other accessory Bi, Te, Cu and Pb minerals are present and include krupkaite and hedleyite as inclusions in schirmerite. Krupkaite ($PbCuBi_3S_6$) occurs as very small grains, always enclosed by schirmerite. Its occurrence is confirmed by SEM–EDX. Hedleyite (Bi_2Te_3) occurs as small (<10 μm) inclusions in schirmerite (Fig. 7C). Hedleyite is the only telluride found in the investigated samples.

Freibergite ($(Ag, Cu, Fe, Zn)_{12}(Sb, As)_4S_{13}$) occurs as inclusions in galena or on grain margins of chalcopyrite.

Tennantite ($(Cu, Ag, Zn, Fe)_{12}As_4S_{13}$) and Tetrahedrite ($(Cu, Fe, Ag, Zn)_{12}Sb_4S_{13}$) occur as relatively coarse grains, enclosed in chalcopyrite or occur on the grain margins of chalcopyrite, in spatial association with sphalerite (Fig. 6D) and/or galena (Fig. 6.B). Tennantite is the most abundant mineral of this group in the deposit and one analysis (Table 1) reveals a small content (4.77 wt.% Sb).

Ag–Au Amalgam is observed in intimately association with matildite (Fig. 7F). The SEM–EDX analyses of this amalgam show concentrations ranging from 65.73 to 74.91 wt.% Ag, and 25.09 to 34.27 wt.% Au (Table 2).

Anglesite ($PbSo_4$) represents a supergene alteration of galena. The alteration to anglesite starts mostly at the rims of galena grains.

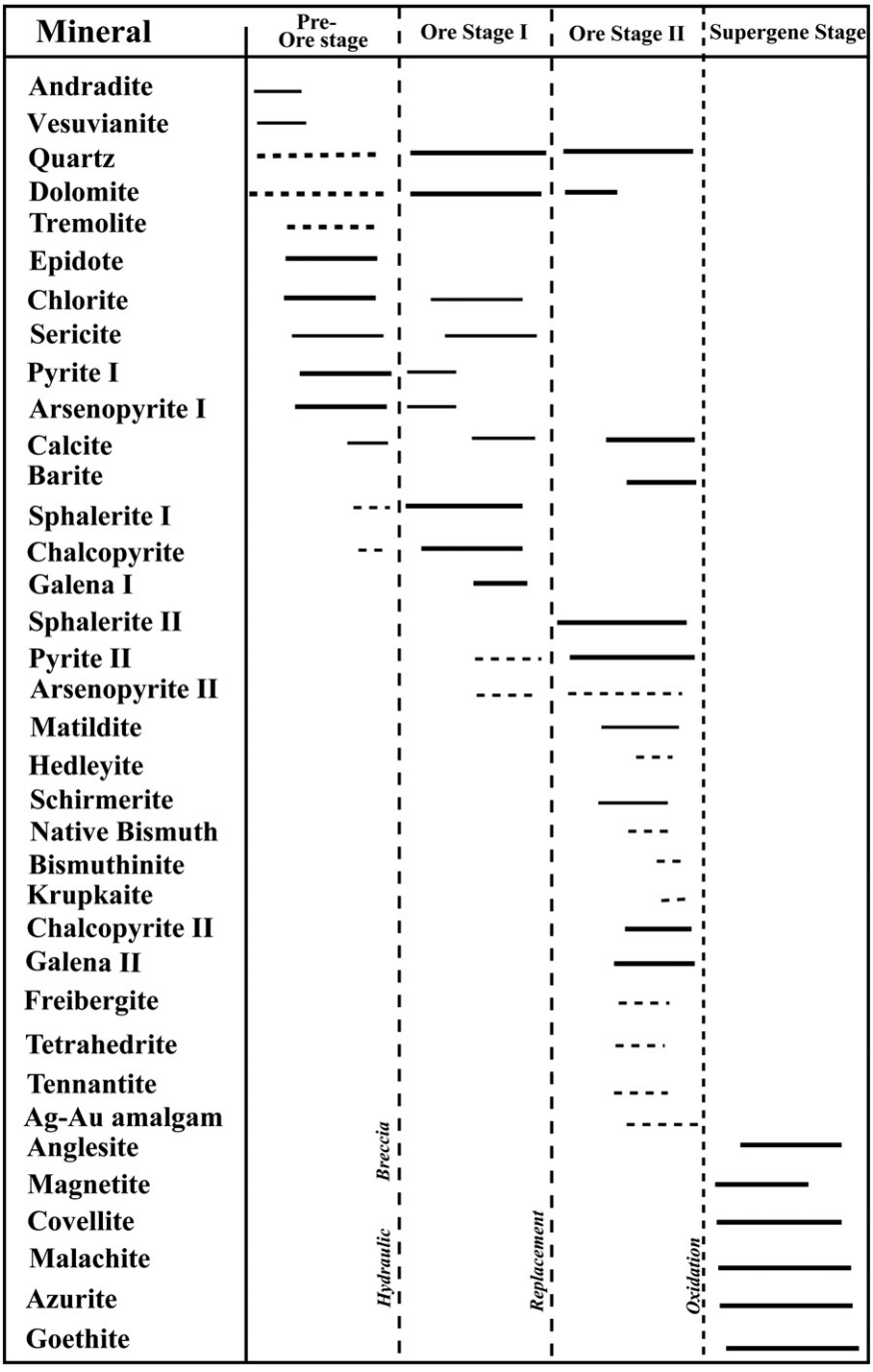

Fig. 8. Paragenetic sequence of the mineralization from the Amensif ore deposit.

Covellite (CuS), Malachite ($Cu_2(CO_3)(OH)_2$), Azurite ($Cu_3(CO3)_2(OH)_2$), and iron hydro-oxides are the secondary minerals resulting from supergene alteration of chalcopyrite and pyrite.

5.2.2. Paragenetic sequence

Ilmen et al. (2014b) established a paragenetic sequence of mineralization in the Amensif deposit. These authors defined two ore stages preceded by a pre-ore (gangue) stage that consists of formation of the mineral gangue and these ore stages are followed by a supergene stage (Fig. 8). In this paper we amend this paragenetic sequence.

Briefly, the pre-ore stage is marked by the formation of hydrothermal minerals: calcite, dolomite, andradite, vesuvianite, quartz, chlorite, tremolite, sericite and pyrite.

The first ore stage is marqued by formation of early pyrite, arsenopyrite and early sphalerite (I) with minor of galena (I). Formation of these minerals is accompanied by crystallization of quartz and calcite.

The second ore stage involved formation of sulphides. In decreasing order of abundance, they are chalcopyrite, sphalerite, galena, pyrite, arsenopyrite and tetrahedrite–tennantite. This stage is chiefly characterized by strong replacement textures among sulphide minerals. An important replacement of the early sphalerite and galena by chalcopyrite, tetrahedrite–tennantite, late pyrite (II) and late arsenopyrite (II) is observed. Late sphalerite (II) appears with blebs of chalcopyrite or entirely replaced by chalcopyrite and galena (II). Pyrite and arsenopyrite are partially or entirely replaced by chalcopyrite. In contrast to the first stage, late pyrite (II) and arsenopyrite (II) occur in fine-grained size aggregates. This reduction in grain size reflects a change in thermo-barometric conditions. Formation of fine arsenopyrite grains probably enriched in gold seems to occur in oversaturated hydrothermal solutions with S–As-containing complex compounds of gold, whose decomposition results in a great number of sulphide seeds, which rapidly crystallize (Volkov et al., 2006). The commonly observed occurrence of paragenesis of arsenopyrite in pyrite-containing sedimentary rocks and the over growth of high-Au arsenopyrite on globular-crystalline pyrite aggregates are the evidence for the crucial role of syngenetic pyrite in the deposition of gold-containing arsenopyrite (Kovalev et al., 2011). In the Amensif deposit, chalcopyrite replaces pyrite and arsenopyrite. Matildite and schirmerite crystallize before native bismuth, followed by bismuthinite, krupkaite, hedleyite, and galena which replace all these phases. Tennantite, tetrahedrite and freibergite were formed after formation of galena. Gold is present as inclusions in arsenopyrite and as Ag–Au amalgam associated with galena. Silver is mainly hosted by matildite, schirmerite, tennantite–tetrahedrite, freibergite, and Ag–Au amalgam. This stage is identified based on the replacement relationship observed between sulphide minerals.

5.3. Geochemistry

Chemical analyses of all above-mentioned ore minerals are given in Tables 1, 2 and 3. One out of five arsenopyrite analyses contains 2.74 wt.% Sb. The zinc ores are composed of two types: iron-rich sphalerite (6 analyses) containing 3.1–10.53 wt.% Fe and iron-poor sphalerite (5 analyses) (28–40 wt.% Fe and 59–69 wt.% S). The analysed chalcopyrite, galena and pyrite lacked SEM-detectable trace elements. One analysis each of tennantite and freibergite yielded respectively, 12.75 and 32.74 wt.% Ag in 9 analyses. Silver is often carried by the matildite 25 to 31 wt.% Ag. Schirmerite contains 5–8 wt.% Ag in 6 analyses. Minor amounts of native bismuth, bismuthinite, hedleyite and krupkaite were identified in close association with galena and matildite. Gold is observed as an Ag–Au amalgam. Three analyses yielded 65.73–69.59 wt.% Ag and 30.41–34.27 wt.% Au (Table 2).

Massive chalcopyrite–sphalerite–galena with lesser silver-gold is the commercial ores exploited since mining operations began. Copper is the most abundant metal followed by zinc then lead. The potential for significant Cu–Pb–Zn ore in the deposit has been tested by drill programmes since 2011. Ore reserves are ca. 0.5 Mt with grades of 3.21% Zn, 0.58% Pb, 0.86% Cu, 83.3 ppm Ag, and 0.41 ppm Au (Ilmen et al., 2014b).

5.4. Lead isotopes

Lead isotope data can be used to help define the probable source material (2 samples) of the ore lead. On the basis of the lead isotopic data for Amensif and Tighardine ores (25 km east of Amensif) ($^{206}Pb/^{204}Pb$ (18.053–18.324), $^{207}Pb/^{204}Pb$ (15.534–15.577), and $^{208}Pb/^{204}Pb$ (37.780–37.986)), the metallogenic episode that give rise to the polymetallic mineralization of Amensif is attributed to the Cambro–Ordovician volcanic event (Ilmen et al., 2014b). In the $^{206}Pb/^{204}Pb$ versus $^{207}Pb/^{204}Pb$ diagram (Fig. 9), galena Pb isotope ratios for Amensif plot between the mantle and the upper crustal curves, close to the orogene one of the Zartman and Doe curve (Doe and Zartman, 1979; Zartman and Doe, 1981; Megaw, 1998), consistent with a dominantly upper crustal reservoir with significant contribution of the mantle lead. These data (2 analyses) show clearly that Pb in the ore fluid was a mixture of upper crustal Pb and mantle Pb. During this period, a carbonate platform developed and was accompanied by an intense volcanic activity with local substitution of the carbonate facies by volcano-sedimentary rocks. Field and laboratory observations suggest that ore forming materials were derived from the Cambro–Ordovician volcanic series. The Cambro–Ordovician formations from the surrounding area (Assif El Mal (Bouabdellah et al. 2009); Azegour (Badra, 1993)) are characterized by strong mafic lavas and volcanic to pyroclastic rocks.

The probable source of lead mineralization in Assif El Mal is related to upper crustal reservoir, including Hercynian granitoids (Bouabdellah et al. 2009). The lead isotopic data from Assif El Mal deposit, 20 km NW of Amensif, plot between the orogene and upper crust curves (Bouabdellah et al. 2009). These authors considered that the Assif El Mal Pb–Zn- (Cu–Ag) veins are related to the Jurassic intrusive complex

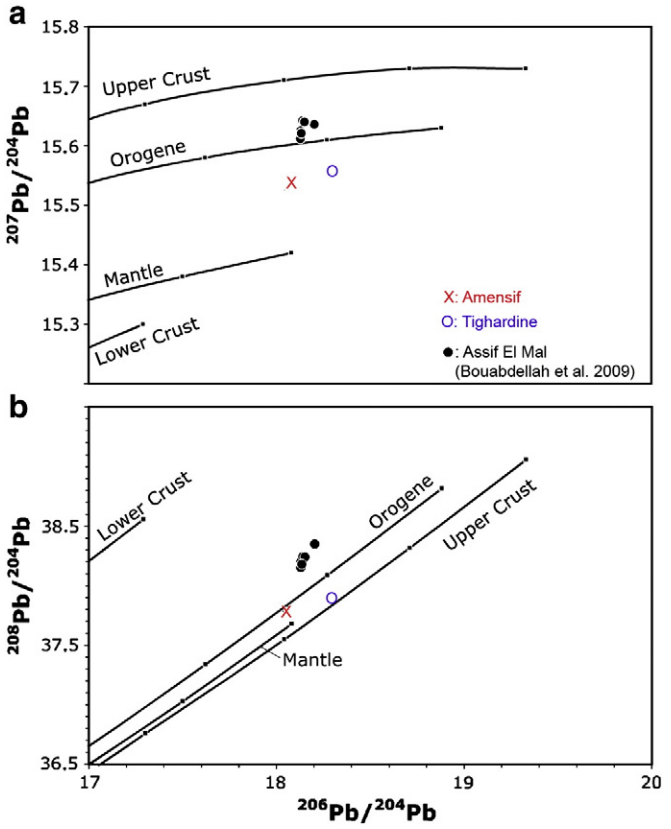

Fig. 9. Comparison of Amensif and Tighardine galena isotope compositions (Ilmen et al., 2014b) to those of galena from the Assif El Mal deposit (Bouabdellah et al. 2009). Curves from Zartman and Doe (1981).

of gabbro to diorite compositions coincident with the beginning of Central Atlantic rifting (Bouabdellah et al., 2009).

6. Discussion

The Amensif carbonate-replacement mineralization is one of several hydrothermal ore types (skarn, manto-type, auriferous shear zone,) in the Guedmiwa district of the western High Atlas Mountains which are probably associated with Permian granitic plutons.

Although some carbonate-replacement deposits in Guedmiwa district are located distal to the Azegour granite, lead isotope composition of galena indicates a mantle contribution to the Amensif system (Ilmen et al., 2014b). The intimate relationship between bismuthinite, schirmerite, matildite, krupkaite, hedleyite, native bismuth, Ag–Au amalgam, galena, sphalerite with chalcopyrite disease, andradite, vesuvianite, tremolite, chlorite, quartz and barite at the Amensif, provides strong evidence for the proximity of mineralization to a magmatic source (Meinert et al., 2003; Voudouris et al., 2008). In addition, the spatial relationship of sulphides with the Permian rhyolitic dikes is also consistent with the involvement of magmatic components in the ore system. Thus, the mineralization of Amensif is probably genetically related to the two contrasting magmatic events recognized in the western High Atlas: (i) the Cambro–Ordovician volcanic event and (ii) the Permian magmatic event.

Besides its close relationship with native gold in the Talat n'Imjjad shear zone (Ilmen et al., 2014a), Bi is also intimately associated with Ag in the Amensif deposits. The mineralization observed in different types of samples from the Amensif deposit has very similar Cu–Pb–Bi–Ag–Sb–Te geochemical signature, which is the main argument to relate them to the magmatic system. According to Foord and Shawe (1989) and Voudouris et al. (2008), matildite occurs in the absence of galena, intergrown, for example, with aikinite, wittichinite and emplectite. They attributed its formation to the breakdown of chalcopyrite, with Bi and some Pb and Ag being incorporated within the matildite lattice at temperature less than 220 °C. Galena from Amensif contains tennantite, tetrahedrite and freibergite inclusions. According to Malakhov (1968) and Foord and Shawe (1988), the presence of minor amounts Ag and Sb with Bi in galena from Kamariza (Greece) is the result of its formation at relatively low temperature (Voudouris et al., 2008). It is known today that galena from hydrothermal deposits contains anomalous and significant levels of Bi, Ag, Sb, Te, Se, Cu, Tl and Zn (Foord and Shawe, 1989). Under most conditions Bi–Te–Sb-bearing minerals are suitable indicators of the presence of these elements, being particularly useful in geochemical exploration for gold and silver (Malakhov, 1968; Boyle and Jonasson, 1984; Ciobanu et al., 2009).

7. Conclusions

- ã The Amensif ore deposit formed by a carbonate replacement system that developed in Lower Cambrian carbonates cut by a swarm of Permian rhyolitic dikes.
- ã The mineralization formed distal to the Azegour granite (Permian, 271 ± 3 Ma; Mrini et al., 1992). Differences and similarities among the geological setting, mineralogy, paragenesis, and alteration features of carbonate replacement mineralization suggest that the hydrothermal system is probably related to the Permian magmatic event which is the precursor of leaching of Cambro–Ordovician volcanic rocks.
- ã The Amensif Cu–Pb–Zn–Ag-(Au) mineralization is lithologically and tectonically controlled. Structural control is particularly evident since the deposit is positioned at the intersection of the ENE–WSW-trending Erdouz fault and the WNW–ESE-trending Al Medinet fault.
- ã Ore minerals consist mainly of sulphides (chalcopyrite, pyrite, sphalerite, galena) and sulpho-arsenides (arsenopyrite), native metals (Bi, Ag–Au), and sulphosalts and sulpho-bismuthinides of Ag, Bi, Cu, Pb and Te. The presence of Ag and Au minerals is not revealed in this assemblage, but these precious metals occur in considerable amounts in other ore minerals, principally tetrahedrite, tennantite, freibergite, matildite, schirmerite and Ag–Au amalgam. Additionally, minor amounts of Te and Bi form fine-grained hedleyite. Sphalerite shows the chalcopyrite disease of Barton and Bethke (1987).
- ã Hydrothermal alteration surrounding the orebodies has resulted in an alteration assemblage of dolomite, saddle dolomite, Mn-dolomite, calcite, barite, ankerite, chlorite, tremolite, andradite, vesuvianite, and quartz.
- ã The presence of chalcopyrite disease indicates high-temperature conditions of ore deposition (Barton and Bethke, 1987). Thus, it can be suggested that this paragenesis formed under high to medium temperature hydrothermal conditions, from a complex Cu–Pb–Zn–Bi–Sb–S–Ag–Au–Te-bearing fluid (Ilmen et al., 2014b). The matildite newly discovered at the Amensif deposit in close association with galena suggests high temperature conditions of galena–matildite solid solution. Craig (1967), Nedachi et al. (1973), and Foord and Shawe (1989) have concluded that most mineral assemblages belonging to the Ag–(Cu)Pb–Bi–S system have crystallized at temperature between 200 and 400 °C.
- ã The enrichment of Bi, Te, Sb and Pb in the mineralization at Amensif suggests a magmatic contribution to the ore-forming fluid. According to Ciobanu et al. (2006), the presence of Te-minerals in an ore, such as hedleyite at Amensif, is indicative of a magmatic signature. Bismuth minerals also have been considered pathfinders for Au in a variety of deposit types (skarn, stringer zone of VMS, intrusion-related Au; Ciobanu et al. 2009). Our study confirms the earlier suggestion that, in the Amensif deposit, the Cu–Pb–Zn mineralization is a carbonate replacement type. In the presence of Bi, large amounts of Ag can be accommodated in the structure of galena.
- ã Preliminary lead isotopic data suggest that the ore-forming components were derived from a mixture of upper crustal and mantle material (Ilmen et al., 2014b). On the basis of this preliminary lead isotopic data, we suggest that the hydrothermal fluid related to Permian granite leached metals from the Cambro–Ordovician rocks and deposited these in the carbonate host rocks.
- ã The Amensif deposit is a typical example of a distal skarn, and is compatible with a model for polymetallic carbonate replacement type mineralization.

Acknowledgements

This study is part of a PhD thesis of the first author on the metallogeny of the western High Atlas belt. This work has been financed by Guemassa Mining Company (Managem Group) and DLGR Laboratory (Cadi Ayyad University, Marrakech). The authors thank the Reminex Center of Marrakech for help during this study. Prof. P. Voudouris, Prof. John F. Slack and Prof. Mohammed Bouabdellah are gratefully acknowledged for their constructive comments, suggestions and linguistic improvements.

References

Alansari, A., Bajddi, A., Zouhair, M., 2009. Mise en évidence d'une évolution verticale dans la minéralogie et la typologie des minéralisations à Cu–Zn–Pb–Ag–Ba de tighardine : apports à l'exploration minière dans le Haut Atlas occidental (Maroc). Notes et Mémoires du Service Géologique Rabat, Maroc 530, pp. 31–44.

Arribas, A., 1995. Characteristics of high-sulfidation epithermal deposits, and their relation to magmatic fluid. In: Thompson, J.F.H. (Ed.), Magmas, Fluids and Ore Deposits. Mineralogical Association of Canada, Short Course Series 23, pp. 419–454.

Badra, L., 1993. Les minéralisations polymétalliques (Pb–Zn–Cu, Ba) du Haut-Atlas Occidental marocain et de ses confins dans leurs cadre géodynamique Unpublished PhD thesis, University of Orléans, France.

Baidada, B., 2012. Etude Gîtologique et Minéralogique de la Zone de Cisaillement Aurifère de Talat n'Imjjad (Région d'Amezmiz, Haut Atlas Occidental, Maroc). Unpublished Master's diplomaCadi Ayyad University, Marrakech, Morocco.

Barton, P.B., Bethke, P.M., 1987. Chalcopyrite disease in sphalerite: pathology and epidemiology. Am. Mineral. 72, 451–467.

Berrada, S.H., Marcoux, E., Hafid, A., 2015. Le skarn Mo–W–Cu à grenat, wollastonite, pyroxène et vésuvianite D'azegour (Haut-Atlas, Maroc). Bull. Soc. Géol. Fr. 186, 21–34.
Bouabdellah, M., Beaudoin, G., Leach, D.L., Grandia, F., Cardellach, E., 2009. Genesis of the Assif El Mal Zn–Pb (Cu, Ag) vein deposit. An extension-related Mesozoic vein system in the High Atlas of Morocco: structural, mineralogical, and geochemical evidence. Mineral. Deposita 44, 689–704.
Boyle, R.W., Jonasson, I.R., 1984. The geochemistry of antimony and its use as an indicator element in geochemical prospecting. J. Geochem. Explor. 20, 223–302.
Bristol, S.K., Spry, P.G., Voudouris, P.C., Melfos, V., Mathurd, R.D., Fornadela, A.P., Sakellarise, G.A., 2015. Geochemical and geochronological constraints on the formation of shear-zone hosted Cu–Au–bi–Te mineralization in the Stanos area, Chalkidiki, northern Greece. Ore Geol. Rev. 66, 266–282.
Calagari, A.A., Hosseinzadeh, G., 2006. The mineralogy of copper-bearing skarn to the east of the Sungun-Chay River, East-Azarbaidjan, Iran. J. Asian Earth Sci. 28, 423–438.
Canet, C.M., Camprubi, A., Gonzalez-Partida, E., Linares, C., Alfonso, P., Pineiro-Fernandez, F., Prol-Ledesma, R.M., 2009. Mineral assemblages of the Francisco I. Madero Zn–Cu–Pb–(Ag) deposit, Zacatecas, Mexico: implications for ore deposit genesis. Ore Geol. Rev. 35, 423–435.
Cepedal, A., Fuertes-Fuente, M., Martin-Izard, A., Gonzalez-Nistal, S., Rodriguez-Pevida, L., 2006. Tellurides, selenides and bi-minerals assemblages from the Rio Narcea Gold belt, Asturias, Spain: genetic implications in Cu–Au and Au skarns. Mineral. Petrol. 87, 277–304.
Ciobanu, C.L., Cook, N.J., 2004. Skarn textures and a case study: the Ocna de Fier-Dognecea Orefield, Banat, Romania. Ore Geol. Rev. 24, 315–370.
Ciobanu, C.L., Cook, N.J., Damian, F., Damian, G., 2006. Gold scavenged by bismuth melts: an example from alpine shear-remobilizates in Highis Massif, Romania. Mineral. Petrol. 87, 351–384.
Ciobanu, C.L., Cook, N.J., Pring, A., Brugger, J., Danyushevsky, L.V., Shimizu, M., 2009. Invisible gold in bismuth chalcogenides. Geochim. Cosmochim. Acta 73, 1970–1999.
Ciobanu, C.L., Birch, W.D., Cook, N.J., Pring, A., Grundler, P.V., 2010. Petrogenetic significance of Au–Bi–Te–S associations: the example of Maldon, central Victorian gold province, Australia. Lithos 116, 1–17.
Cook, N.J., 1997. Bismuth and bismuth-antimony sulphosalts from Neogene vein mineralisation, Baia Borsa area, Maramures, Romania. Mineral. Mag. 61, 387–409.
Cook, N.J., Ciobanu, C.L., 2004. Bismuth tellurides and sulphosalts from the Larga hydrothermal system, Metaliferi Mts., Romania: paragenesis and genetic significance. Mineral. Mag. 68, 301–321.
Cox, D.P., 1986. Descriptive Model of Polymetallic Veins. In: Cox, D.P., Singer, D.A. (Eds.), Mineral Deposit Models: U.S. Geol. Survey Bull., p. 1693
Craig, J.R., 1967. Phase relations and mineral assemblages in the Ag–Bi–Pb–S system. Mineral. Deposita 1, 278–306.
Damian, G., Ciobanu, C.L., Cook, N.J., Damian, F., 2008. Bismuth sulphosalts from the galena–matildite series in the Cremenea vein, Şuior, Baia Mare district, Romania. N. Jahrb. Mineral. Abh. 185, 199–213.
Dias, R., Hadani, M., Machado, L.I., Adnane, N., Hendaq, Y., Madih, K., Matos, C., 2011. Variscan structural evolution of the western High Atlas and the Haouz plain (Morocco). J. Afr. Earth Sci. 61, 331–342.
Doe, B.R., Zartman, R.E., 1979. Plumbotectonics, the Phanerozoic. In: Barnes, H.L. (Ed.), Geochemistry of Hydrothermal Ore Deposits. John Wiley and Sons, New York, pp. 22–70.
Einaudi, M.T., Burt, D.M., 1982. Introduction–terminology, classification, and composition of skarn deposits. Econ. Geol. 77, 745–754.
El Khalile, A., Touil, A., Hibti, M., Bilal, E., 2014. Metasomatic zoning, mineralizations and genesis of Cu, Zn and Mo Azegour skarns (western High Atlas, Morocco). Carpath. J. Earth Environ. Sci. 9, 21–32.
Eldridge, C.S., Bourcier, W.L., Ohmoto, H., Barnes, H.L., 1988. Hydrothermal inoculation and incubation of the chalcopyrite disease in sphalerite. Econ. Geol. 83, 978–989.
Foord, E.E., Shawe, D.R., 1988. Coexisting galena PbS_{ss} and sulfosalts evidence for multiple episodes of mineralization in the Round Mountain and Manharan GoldDistricts in Nevada. Can. Mineral. 26, 355–376.
Foord, E.E., Shawe, D.R., 1989. The Pb–Bi–Ag–Cu-(Hg) chemistry of galena and some associated sulfosalts: a review and some new from Colorado, California and Pennsylvania. Can. Mineral. 27, 363–382.
Fornadel, A.P., Spry, P.G., Melfos, V., Vavelidisb, M., Voudouris, P.C., 2011. Is the Palea Kavala Bi–Te–Pb–Sb–Au district, northeastern Greece, an intrusion-related system? Ore Geol. Rev. 39, 119–133.
Ilmen, S., 2011. Contribution à l'Étude Géologique du Gîte à Cu, Zn, Pb et Ag ± Au D'Amensif (Région d'Azegour-Haut Atlas Occidental) Unpublished Master's diploma Cadi Ayyad University, Morocco.
Ilmen, S., Alansari, A., Bajddi, A., Maacha, L., 2014a. Cu–Au vein mineralization related to the talat n'imjjad shear zone (western High Atlas, Morocco): geological setting, ore mineralogy, and geochemical evolution. Arabian J. Geosci. http://dx.doi.org/10.1007/s12517-014-1503-y.
Ilmen, S., Alansari, A., Bajddi, A., Ennaciri, A., Maacha, L., 2014b. Mineralogical and geochemical characteristics of the Amensif Cu, Pb, Zn, (Ag, Au) ore deposit, western High Atlas, Morocco. J. Tethys 2, 118–136.
Ilmen, S., 2014. Report on the mineralogical studies of the western High Atlas, Morocco (Unpublished report).
Kovalev, K.R., Kalinin, Y.A., Naumov, E.A., Kolesnikova, M.K., Korolyuk, V.N., 2011. Gold-bearing arsenopyrite in eastern Kazakhstan gold-sulfide deposits. Russ. Geol. Geophys. 52, 178–192.
Labriki, M., 1996. Carte géologique du Maroc, feuille d'Amezmiz au 1/100 000. Notes et Mémoires du Service Géologique, Rabat, Maroc 372.
Malakhov, A.A., 1968. Bismuth and antimony in galenas as indicators of some conditions of ore formation. Geochem. Int. 10, 1055–1068.
Marcoux, E., Moëlo, Y., Leistel, J.M., 1996. Bismuth and cobalt minerals as indicators of stringer zones to massive sulphide deposits, Iberian pyrite belt. Mineral. Deposita 31, 1–26.
Megaw, P.K.M., 1998. Carbonate-hosted Pb–Zn–Ag–Cu–Au replacement deposits: an exploration perspective. In: Lentz, D.R. (Ed.), Mineralized Intrusion Skarn Systems. Mineralogical Association of Canada, Short course 26, pp. 337–413.
Meinert, L.D., 1992. Skarns and skarn deposits. J. Geol. Assoc. Can. 19, 145–162.
Meinert, L.D., Hedenquist, J.W., Satoh, H., Matsuhisa, Y., 2003. Formation of anhydrous and hydrous skarn in Cu–Au ore deposits by magmatic fluids. Econ. Geol. 98, 147–156.
Morris, H.T., 1986. Descriptive model of polymetallic replacement deposits. In: Cox, D.P., Singer, D.A. (Eds.), Mineral Deposit Models. U.S. Geological Survey Bulletin 1693, pp. 99–100.
Mrini, Z., Rafi, A., Duthou, J.L., Vidal, P., 1992. Chronologie Rb–Sr des granitoïdes hercyniens du Maroc: conséquences. Bull. Soc. Géol. Fr. 163, 281–291.
Nedachi, M., Takeuchi, T., Yamaoka, K., Taniguchi, M., 1973. Bi–Ag–Pb–S minerals from genosawa mine, Akita Prefecture, Northeastern Japan. Sci. Rep. Tohoku Univ. 12, 69–80.
Permingeat, F., 1957. Le gisement de molybdène, tungstène et cuivre d'Azegour (Haut-Atlas): etude pétrographique et métallogénique. Notes et Mémoires du Service Géologique, Rabat, Maroc 141.
Pouclet, A., Ouazzani, H., Fekkak, A., 2008. The Cambrian volcano-sedimentary formations of the westernmost High Atlas (Morocco): their place in the geodynamic evolution of the West African Palaeo-Gondwana northern margin. Geol. Soc. Lond. 297, 303–327.
Ramdohr, P., 1969. The Ore Minerals and Their Intergrowths. Pergamon Press, Oxford, England.
Volkov, A.V., Genkin, A.D., Goncharov, V.I., 2006. Gold species in ores of the Natalkinskoe and Maiskoe deposits (northeastern Russia). Tikhookean. Geol. 25 (6), 18–29.
Voudouris, P., Melfos, V., Spry, P.G., Bonsall, T.A., Tarkian, M., Solomos, C., 2008. Carbonate-replacement Pb–Zn–Ag–Au mineralization in the Kamariza area, Lavrion, Greece: mineralogy and thermochemical conditions of formation. Mineral. Petrol. 94, 85–106.
Voudouris, P.C., Spry, P.G., Mavrogonatos, C., Sakellaris, G.A., Bristol, S.K., Melfos, V., Fornadel, A.P., 2013. Bismuthinite derivatives, lillianite homologues, and bismuthsulfotellurides as indicators of gold mineralization in the Stanos shear-zone related deposit, Chalkidiki, northern Greece. Can. Mineral. 51, 119–142.
Ye, L., Liu, T., Yang, Y., Wei Gaoa, b., Ziping Pana, c., Tan Bao, T., 2014. Petrogenesis of bismuth minerals in the Dabaoshan Pb–Zn polymetallic massive sulfide deposit, northern Guangdong Province, China. J. Asian Earth Sci. 82, 1–9.
Zartman, R.E., Doe, B.R., 1981. Plumbo-tectonics, the model. Tectonophysics 75, 135–162.
Zerhouni, Y., 1988. Contribution à l'étude géologique de la région d'Azegour et des minéralisations en Mo, W, Cu et Fe. Haut-Atlas de Marrakech-MarocCadi Ayyad University, Morocco Unpublished Ph.D. thesis.